Central European Journal of Energetic Materials
ISSN 1733-7178; e-ISSN 2353-1843

Cent. Eur. J. Energ. Mater. 2017, *14*(4): 888-916; DOI: 10.22211/cejem/71193

Decomposition Pathways for Aqueous Hydroxylammonium Nitrate Solutions: a DFT Study

Yu-ichiro Izato,* Mitsuo Koshi, Atsumi Miyake

Yokohama National University,
79-7 Tokiwadai, Hodogaya-ku, 240-8501 Yokohama (KANAGAWA), Japan
**E-mail: izato-yuichiro-hk@ynu.jp*

Abstract: Hydroxylammmonium nitrate (hydroxylamine nitrate, HAN) is one of the most promising candidates as a replacement for commonly used liquid mono-propellants such as hydrazine. The reaction pathways involved in the initial and the catalytic decomposition of HAN in aqueous solution were determined using quantum chemistry calculations incorporating solvent effects. Optimized structures were obtained for the reactants, products and transition states at the ωB97XD/6-311++G(d,p)/SCRF = (solvent = water) level of theory and the total electron energies of these structures were calculated at the CBS-QB3 level of theory. In the initial decomposition, the ion-neutral NH_3OH^+-HNO_3 reaction, the neutral-neutral NH_3O-HNO_3 reaction and the HNO_3 self-decomposition pathways were all found to have reasonable energy barriers, with values of 91.7 kJ/mol, 88.7 kJ/mol and 89.8 kJ/mol, respectively. The overall reaction resulting from any of these pathways can be written as: HAN → HONO + HNO + H_2O. The ionic reaction is dominant during the initial decomposition of HAN in aqueous solution because NH_3OH^+ and NO_3^- are the major species in such solutions. We also developed six catalytic mechanisms and each of these schemes provided the same global reaction: NH_2OH + HONO → N_2O + $2H_2O$. The *t*-$ONONO_2$ oxidizing scheme is the most plausible based on the energy barrier results.

Keywords: hydroxylamine nitrate, reaction pathway, liquid-phase reaction, density functional theory

1 Introduction

Hydroxylammonium nitrate (hydroxylamine nitrate, HAN), having the chemical formula $[NH_3OH]^+[NO_3]^-$, is one of the most promising candidates as a replacement for commonly used liquid mono-propellants such as hydrazine [1-3]. As such, there have been many experimental and theoretical studies concerning the combustion behaviour of the so-called next generation HAN-based propellants [4-11]. Previous research has demonstrated that some HAN-based solutions exhibit extremely high burning rates, and this property has limited the usefulness of such solutions in certain applications [3-6] because overly high burning rates can sometimes lead to serious accidents [12-14]. Therefore, the development of advanced techniques to control the combustion of HAN-based propellants is essential.

A detailed chemical reaction model is a helpful step in any investigation of rapid transient phenomena such as propellant ignition and flame extinction. Khare *et al*. [15] studied the ignition behaviour of HAN/water solutions and developed a theoretical model incorporating gas [16, 17] and condensed phase reactions that include electrolysis of ionic liquids and the Lee and Litzinger model [18]. This prior work calculated the ignition delay of aqueous HAN solutions using the model and discussed the appropriateness of electrolytically-induced ignition systems for HAN-based propellants. The Lee and Litzinger model [18] consists of the following eight reactions:

$$HAN + H_2O \rightleftharpoons NH_2OH + HNO_3 + H_2O \quad (1)$$
$$NH_2OH + HNO_3 \rightleftharpoons HONO + HNO + H_2O \quad (2)$$
$$NH_2OH + HONO \rightleftharpoons N_2O + 2H_2O \quad (3)$$
$$2HNO \rightleftharpoons N_2O + H_2O \quad (4)$$
$$NH_2OH + HNO \rightleftharpoons N_2 + 2H_2O \quad (5)$$
$$3HONO \rightleftharpoons 2NO + HNO_3 + H_2O \quad (6)$$
$$HNO + HNO_3 \rightleftharpoons 2HONO \quad (7)$$
$$HONO + HNO_3 \rightleftharpoons 2NO_2 + H_2O \quad (8)$$

Lee and Litzinger [18] developed a reduced reaction model based on previously proposed reaction mechanisms [19, 20], and were able to predict the reaction rates by simulating the experimental decomposition process and applying an inverse analysis technique.

The aim of the present study was to gain a better understanding of the chemical reactions of HAN during its initial and catalytic decomposition, and to develop a detailed reaction model on the basis of an *ab initio* study. To this

end, we conducted thermal assessments using *ab initio* quantum chemistry calculations, which are helpful with regard to determining which reactions can be excluded from the mechanism based on thermodynamic arguments. As an example, if a reaction is found to be highly endothermic, or considerably more endothermic than a competing pathway, then that reaction may be safely omitted from the mechanism. This paper presents a detailed reaction scheme for HAN decomposition.

2 Computational

The geometries of the reactants, products, and transition states were optimized at the ωB97XD/6-311++G(d,p) level [21] of theory using the Gaussian 09 program package [22]. Gordon *et al*. [21] developed the ωB97XD method, which includes empirical dispersion forces and is believed to be reliable when applied to systems with weak van der Waals forces. This group also reported that the ωB97XD method yields satisfactory accuracy for kinetics and non-covalent interactions. During the computations, transition states (TSs) were extensively searched for, and, if found, an intrinsic reaction coordinate (IRC) calculation was conducted in order to assign reactants and products to the TS. The energies of the corresponding molecules were evaluated at the CBS-QB3 [23] level of theory, since this is a reasonable time-expense complete basis method. In this study, the geometries and frequencies were calculated at the ωB97XD/6-311++G(d,p) level, the optimized geometries were fixed with no changes allowed and the energies were calculated using the CBS-QB3 method. Solvent effects were included by applying the self-consistent reaction field (SCRF) and polarizable continuum model (PCM) options [24] within the program when investigating the liquid reactions in water.

3 Results and Discussion

Important reactions occurring in the HAN decomposition and the associated energy barriers and energy changes calculated at the CBS-QB3//ωB97XD/6-311++G(d,p)/SCRF = (solvent = water) level of theory are summarized in Tables 1 and 2. Figure 1 depicts the important chemical species during the decomposition.

Table 1. Important reactions in the decomposition of HAN with thermodynamic parameters calculated at the ωB97XD/6-311++G(d,p)/SCRF = (solvent = water) and CBS-QB3//ωB97XD/6-311++G(d,p)/SCRF = (solvent = water) levels of theory

No.	Reaction	ωB97XD /6-311++G(d,p)		CBS-QB3// ωB97XD /6-311++G(d,p)	
		$\Delta E_0^{\ddagger}$ [1]	$\Delta_r E_0$ [2]	$\Delta E_0^{\ddagger}$ [1]	$\Delta_r E_0$ [2]
R1	$HNO_3 \rightleftharpoons OH + NO_2$	no TS	192.3	no TS	205.0
R2	$NH_2OH + HNO_3 \rightleftharpoons NH_2(O)OH + HNO_2$ (TS1)	183.1	73.0	186.5	69.4
R3	$NH_2OH + HNO_3 \rightleftharpoons NH_2(O)NO_2 + H_2O$ (TS2)	125.1	−13.9	124.8	−15.0
R4	$NH_2(O)NO_2 \rightleftharpoons HONO + HNO$ (TS3)	51.3	−15.4	53.1	−29.8
R5	$NH_2(O)NO_2 + H_2O \rightleftharpoons HONO + HNO$ (TS4)	7.0	−15.4	17.0	−29.8
R6	$NH_3O + HNO_3 \rightleftharpoons NH_2ONO_2 + H_2O$ (TS5)	91.9	−55.3	88.7	−83.5
R7	$NH_2ONO_2 \rightleftharpoons HONO + HNO$ (TS6)	57.2	−24.9	88.6	−11.3
R8	$NH_2ONO_2 + H_2O \rightleftharpoons HONO + HNO$ (TS7)	31.2	−24.9	65.2	−11.3
R9	$NH_3OH^+ + HNO_3 \rightleftharpoons [NH_2OH\text{-}NO_2\text{-}H_2O]^+$ (TS8A)	95.1	91.9	91.7	73.7
R10	$[NH_2OH\text{-}NO_2\text{-}H_2O]^+ \rightleftharpoons NH_2(OH)NO_2^+ + H_2O$ (TS8B)	15.1	−59.6	10.4	−45.0
R11	$NH_3OH^+ + HNO_3 \rightleftharpoons [NH_2OH\text{-}NO_2\text{-}H_2O]^+$ (TS9A)	94.1	91.1	94.2	70.2
R12	$[NH_2OH\text{-}NO_2\text{-}H_2O]^+ \rightleftharpoons NH_2(OH)NO_2^+ + H_2O$ (TS9B)	9.9	−58.8	3.8	−41.6
R13	$NH_2(OH)NO_2^+ + NO_3^- \rightleftharpoons NH(OH)NO_2 + HNO_3$	no TS	-124.0	no TS	−128.2
R14	$NH(OH)NO_2 \rightleftharpoons NH(O)N(O)OH$ (TS10)	77.4	76.6	68.9	66.1
R15	$NH(O)N(O)OH \rightleftharpoons HONO + HNO$ (TS11)	63.5	−18.8	65.5	−24.8
R16	$NH(OH)NO_2 + H_2O \rightleftharpoons NH(O)N(O)OH + H_2O$ (TS12)	60.2	76.6	63.3	66.1
R17	$NH(OH)NO_2 \rightleftharpoons NH_2(O)NO_2$ (TS13)	237.1	73.1	233.1	71.1
R18	$NH(OH)NO_2 + H_2O \rightleftharpoons NH_2(O)NO_2 + H_2O$ (TS14)	114.4	73.1	117.4	71.1
R19	$HNO_3 + HNO_3 \rightleftharpoons N_2O_5 + H_2O$ (TS15)	91.6	52.9	89.8	40.1
R20	$NH_2OH + N_2O_5 \rightleftharpoons NH_2O\text{-}NO_2 + HNO_3 + H_2O$ (TS16)	11.2	-140.0	27.5	−126.2
R21	$NH_3OH^+ + N_2O_5 \rightleftharpoons NH_2OH\text{-}NO_2^+ + HNO_3 + H_2O$ (TS17)	64.6	−20.6	50.9	−11.4

[1] Energy barrier in the forward direction [kJ/mol]; [2] Total energy change of reaction [kJ/mol]

Table 2. Important reactions in the HAN/HONO catalytic decomposition with thermodynamic parameters calculated at the ωB97XD/6-311++G(d,p)/SCRF = (solvent = water) and CBS-QB3//ωB97XD/6-311++G(d,p)/SCRF = (solvent = water) levels of theory

No.	Reaction	ωB97XD /6-311++G(d,p)		CBS-QB3// ωB97XD /6-311++G(d,p)	
		$\Delta E_0^{\ddagger}$ [1]	$\Delta_r E_0$ [2]	$\Delta E_0^{\ddagger}$ [1]	$\Delta_r E_0$ [2]
R22	$NH_2OH + HONO \rightleftharpoons NH_2(O)NO + H_2O$ (TS18)	64.9	45.2	74.9	35.3
R23	$NH_2(O)NO \rightleftharpoons 2HNO$ (TS19)	103.4	49.4	80.4	41.8
R24	$NH_2OH + HONO \rightleftharpoons [NH(OH)\text{-}ON] + H_2O$ (TS20)	157.9	144.3	171.2	70.1
R25	$[NH(OH)\text{-}ON] \rightleftharpoons 2HNO$ (TS21)	−5.5	−49.7	16.2	7.0
R26	$NH_3OH^+ + HONO \rightleftharpoons [NH_2OH\text{-}NO\text{-}H_2O]_I^+$ (TS22A)	21.2	26.0	23.6	24.8
R27	$[NH_2OH\text{-}NO\text{-}H_2O]_I^+ \rightleftharpoons NH_2(OH)NO^+ + H_2O$ (TS22B)	17.7	−8.3	9.8	−9.6
R28	$NH_3OH^+ + HONO \rightleftharpoons [NH_2OH\text{-}NO\text{-}H_2O]_{II}^+$ (TS23A)	22.6	24.9	22.6	21.1
R29	$[NH_2OH\text{-}NO\text{-}H_2O]_{II}^+ \rightleftharpoons NH_2(OH)NO^+ + H_2O$ (TS23B)	15.5	−7.2	9.0	−5.9
R30	$NH_2(OH)NO^+ + NH_2OH \rightleftharpoons NH(OH)NO + NH_3OH^+$	no TS	−85.9	no TS	−76.5
R31	$NH_2(OH)NO^+ + NO_3^- \rightleftharpoons NH(OH)NO + HNO_3$	no TS	−90.5	no TS	−90.0
R32	$NH(OH)NO \rightleftharpoons N_2O + H_2O$ (TS24)	234.1	−209.6	222.3	−236.0
R33	$NH(OH)NO + H_2O \rightleftharpoons N_2O + 2H_2O$ (TS25)	94.8	−209.6	95.8	−236.0
R34	$HNO_3 + HONO \rightleftharpoons t\text{-}ONONO_2 + H_2O$ (TS26)	11.2	10.3	11.4	3.0
R35	$HNO_3 + HONO \rightleftharpoons N_2O_4 + H_2O$ (TS27)	124.1	−20.1	128.5	−22.4
R36	$NH_2OH + t\text{-}ONONO_2 \rightleftharpoons NH_2(O)NO + HNO_3$ (TS28)	−48.4	−78.5	−44.8	−64.3
R37	$NH_3OH^+ + t\text{-}ONONO_2 \rightleftharpoons NH_2(OH)NO^+ + HNO_3$ (TS29)	42.1	7.4	26.6	12.2
R38	$HONO + HONO \rightleftharpoons N_2O_3 + H_2O$ (TS30)	45.3	−6.3	50.4	−10.3
R39	$NH_2OH + N_2O_3 \rightleftharpoons [NH_2(O)NO\text{-}HONO]$ (TS31A)	−1.0	26.1	−1.7	1.0
R40	$[NH_2(O)NO\text{-}HONO] \rightleftharpoons NH(OH)NO + HNO_2$ (TS31B)	−31.3	−67.6	−2.7	−29.4
R41	$NH_3OH^+ + N_2O_3 \rightleftharpoons [NH_2(OH)NO\text{-}HONO]^+$ (TS32A)	25.9	31.3	33.9	34.4
R42	$[NH_2(OH)NO\text{-}HONO]^+ \rightleftharpoons NH_2(OH)NO^+ + HONO$ (TS32B)	24.1	−7.3	16.0	−9.0

[1] Energy barrier in the forward direction [kJ/mol]; [2] Total energy change of reaction [kJ/mol].

Reaction R1 in Table 1 is the HO−N bond cleavage of HNO_3 and, following this cleavage, a high speed radical chain reaction develops. Since the activation energy for the homolysis of HNO_3 is very high (205.0 kJ/mol) this represents the rate-controlling step for the radical chain reaction. Therefore, reactions that have a higher energy barrier value than that for cleavage of HNO_3 are omitted as candidates for the thermal decomposition reaction of HAN in the condensed phase.

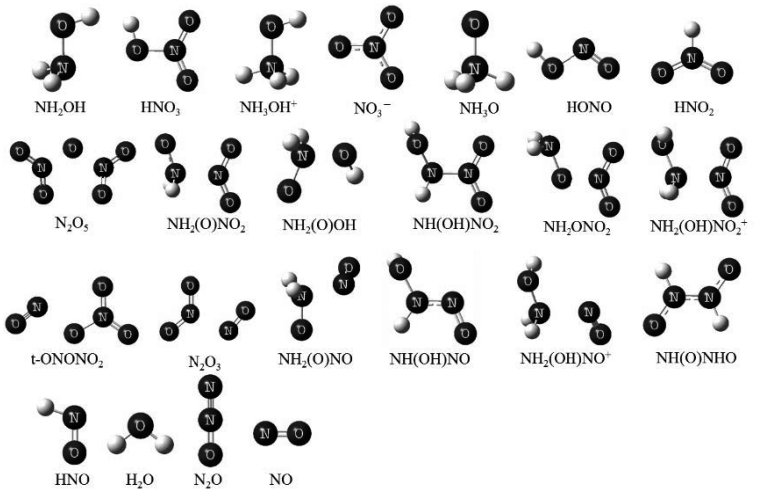

Figure 1. Chemical structures of reactants, products and intermediates involved in HAN decomposition as optimized using the ωB97XD/6-311++G(d,p) level of theory

3.1 The initial decomposition

3.1.1 The neutral-neutral reaction of NH_2OH and HNO_3

This work identified and investigated three neutral-neutral reaction pathways, two of which begin with neutral NH_2OH and HNO_3 molecules. These two pathways are associated with the following chemical reactions:

$$NH_2OH + HNO_3 \rightarrow NH_2(O)OH + HNO_2 \quad (R2)$$
$$NH_2OH + HNO_3 \rightarrow NH_2(O)NO_2 + H_2O \quad (R3)$$

Figure 2 shows the potential energy profiles for these two initial reactions, including the optimized structures of the transition states (TSs) and intermediate complexes. In the mechanism that proceeds *via* TS1, cleavage of the N–OH bond in HNO_3 triggers its decomposition and the resulting OH combines with NH_2OH to form $NH_2(OH)_2$ as the TS. The remaining NO_2 species then removes an H from the $NH_2(OH)_2$ to generate $NH_2(O)OH$ and HNO_2. The energy barrier for this process was calculated to be 186.5 kJ/mol at the CBS-QB3//ωB97XD/6-311++G(d,p)/SCRF = (solvent = water) level of theory.

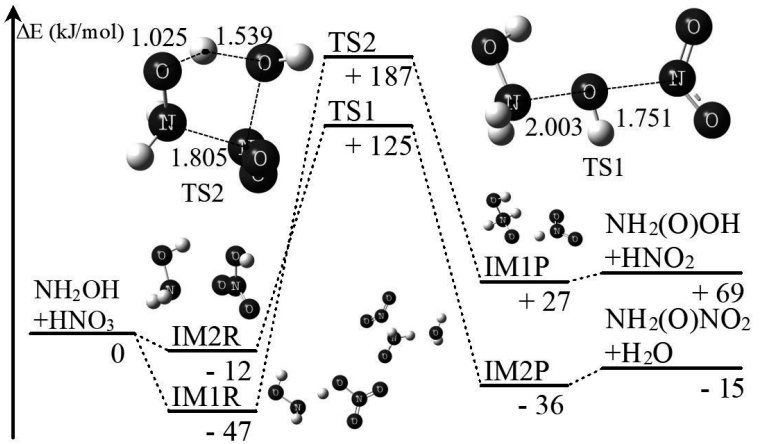

Figure 2. Potential energy profiles* for the bimolecular reaction of NH_2OH and HNO_3

*The energy profiles were calculated at the CBS-QB3//ωB97XD/6-311++G(d,p)/SCRF = (solvent = water) level of theory.

In the mechanism that proceeds *via* TS2, decomposition also begins with cleavage of the N–OH bond in HNO_3, such that the HNO_3 decomposes to OH and NO_2. The OH subsequently subtracts H from NH_2OH to form TS2, while the dissociated NO_2 combines with the $-NH_2$ group in the dehydrogenated NH_2O to form $NH_2(O)NO_2$. The associated energy barrier was determined to be 124.8 kJ/mol. Hence, the R3 process is preferable to R2 on a thermodynamic basis because its energy barrier is lower.

We also investigated the decomposition of $NH_2(O)NO_2$, the product of R3, which proceeds *via* the following reaction:

$$NH_2(O)NO_2 \rightarrow HONO + HNO \quad \text{(R4)}$$

The schematic potential energy profiles of the two possible reaction pathways and optimized structures for the reactants, TSs and products are shown in Figure 3. In one path, $NH_2(O)NO_2$ decomposes to HONO and HNO by intramolecular H transfer to generate TS3, with an energy barrier of 53.1 kJ/mol. In another pathway (R5), water molecules assist in the intramolecular proton transfer (a common effect in many reactions) such that TS4 has a ring structure. In this second scenario, the water catalytic effect decreases the energy barrier to 17.0 kJ/mol. Often in such calculations, the TS in the absence of an explicit solvent effect involves a highly strained ring since the strained ring structure is

necessary to transfer the H from one position in the molecule to another. The result is typically a highly energetic barrier to the reaction. The inclusion of solvent molecules allows the ring structure to be larger in size, thus reducing the ring strain and lowering the transition state energy compared to that required for a smaller cyclic transition state structure. Because both energy barrier heights of the R4 and R5 pathways are much lower than that for R3, the rate determining step is believed to be R3. Although the energy barrier values determined for this neutral-neutral bimolecular reaction are lower than that for HNO_3 cleavage, these values are still much higher than those associated with other mechanisms, as discussed later.

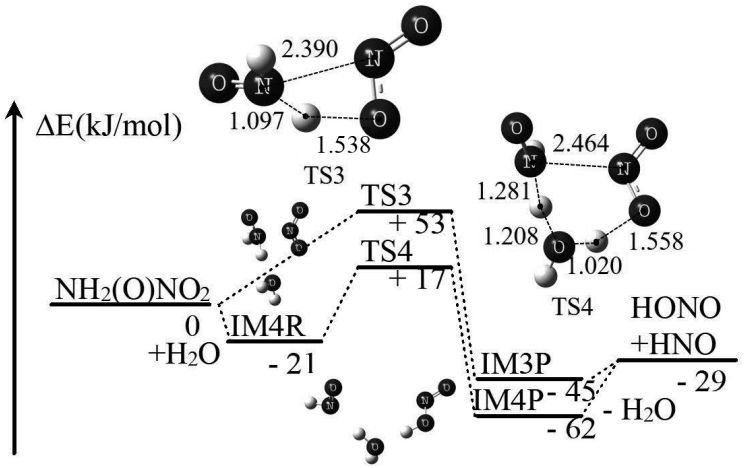

Figure 3. Potential energy profiles* for the decomposition of the intermediate species $NH_2(O)NO_2$

*The energy profiles were calculated at the CBS-QB3//ωB97XD/6-311++G(d,p)/SCRF = (solvent = water) level of theory.

3.1.2 The neutral-neutral reaction of NH_3O and HNO_3

Some theoretical calculations have predicted that the NH_3O isomer is sufficiently stable to be kinetically relevant and may play a key role in many reactions of HAN in aqueous solution [25-28]. Felnadez *et al*. [26] calculated the value for the tautomeric equilibrium between NH_2OH and $^{+}NH_3O^{-}$ in aqueous solution to be $K_T = ([NH_3O]/[NH_2OH]) = 2.6 \times 10^{-2}$, and this isomerization mechanism has been fully investigated on the basis of *ab initio* calculations [27, 28]. We therefore identified and investigated a reaction involving NH_3O and a subsequent reaction as follows:

$NH_3O + HNO_3 \rightarrow NH_2ONO_2 + H_2O$ (R6)

$NH_2ONO_2 (+ H_2O) \rightarrow HONO + HNO (+ H_2O)$ (R7, R8)

Figure 4 depicts the potential energy profile and the optimized structure for the TS and intermediates for this pathway. The decomposition begins with cleavage of the N–OH bond of HNO_3, following which the dissociated OH abstracts H from NH_3O while the NO_2 simultaneously combines with the O− of NH_2O to form TS5. This series of reactions is exothermic and generates H_2O and NH_2ONO_2 with an energy barrier of 88.7 kJ/mol.

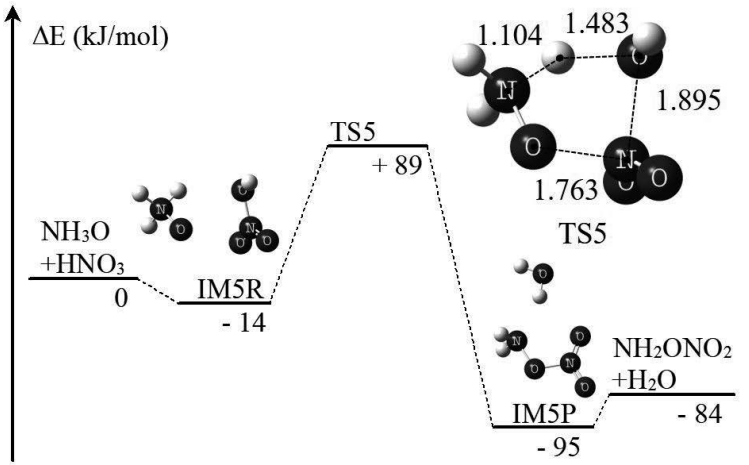

Figure 4. Potential energy profile* for the bimolecular reaction of NH_3O and HNO_3

*The energy profile was calculated at the CBS-QB3//ωB97XD/6-311++G(d,p)/SCRF = (solvent = water) level of theory.

Figure 5 presents the potential energy profiles and the optimized structures for the decomposition of the intermediate species NH_2ONO_2. Here, NH_2ONO_2 decomposes to HONO and HNO by intramolecular H transfer and the presence of water assists this process (R8), just as in R4. The energy barrier was found to be 88.6 kJ/mol, so R6 is considered to be the rate determining step. The maximum energy barrier of the pathway involving NH_3O is the lowest of all of the neutral-neutral bimolecular pathways shown above, indicating that NH_3O plays an important role in HAN decomposition.

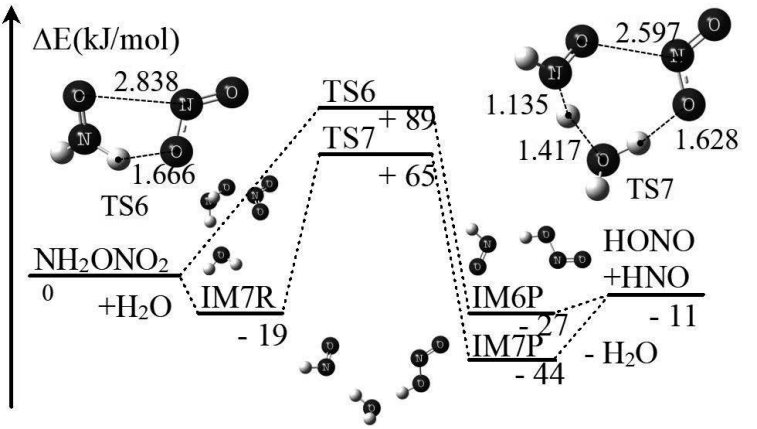

Figure 5. Potential energy profiles* for the decomposition of the intermediate NH_2ONO_2

*The energy profiles were calculated at the CBS-QB3//ωB97XD/6-311++G(d,p)/SCRF = (solvent = water) level of theory.

3.1.3 The ion-neutral reaction of NH_3OH^+ and HNO_3

In aqueous solution, HAN typically dissociates to form the ion pair NH_3OH^+ and NO_3^-. This work therefore examined reactions involving NH_3OH^+ as described below. It should be noted that we were unable to identify any plausible reactions starting with NO_3^- in this study. Figure 6 shows the potential energy profiles and optimized structures for this pathway. This reaction starts with a proton transfer from NH_3OH^+ to HNO_3, after which the protonated $H_2NO_3^+$ decomposes to H_2O and NO_2^+. The NO_2^+ then combines with NH_2OH to form $NH_2(OH)NO_2^+$. The energy barrier was calculated to be 94.2 kJ/mol. The resulting $NH_2(OH)NO_2^+$ is evidently deprotonated by NO_3^-, which is plentiful in aqueous HAN solutions, to give $NH(OH)NO_2$. Thus, the reaction process eventually yields $NH(OH)NO_2$ and H_2O, along with a heat output of 106 kJ/mol.

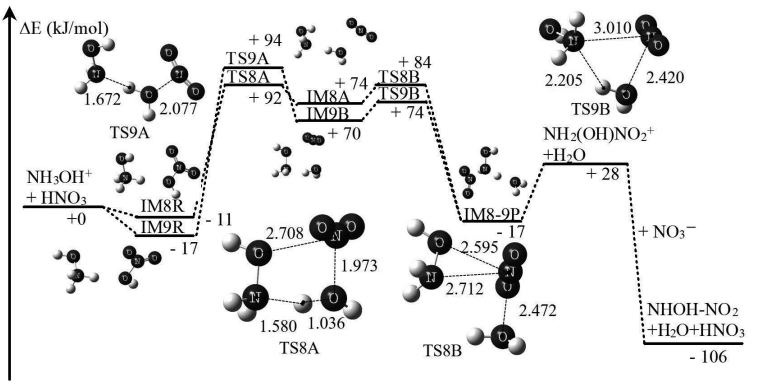

Figure 6. Potential energy profiles* for the bimolecular reaction of NH_3OH^+ and HNO_3

*The energy profiles were calculated at the CBS-QB3//ωB97XD/6-311++G(d,p)/SCRF = (solvent = water) level of theory.

We also assessed the decomposition of the intermediate $NH(OH)NO_2$ as described below.

$$NH_3OH^+ + HNO_3 \rightarrow NH_2(OH)NO_2^+ + H_2O \qquad \text{(R9, R11)}$$

Figure 7 depicts the potential energy profiles and optimized structures for the decomposition of $NH(OH)NO_2$. The decomposition pathways can be roughly separated into two groups. The first consists of pathways that proceed *via* NH(OH)N(O)OH. Here, $NH(OH)NO_2$ transitions to NH(OH)N(O)OH *via* an intermolecular H transfer from −OH to NO_2 to give TS10, after which the N−N bond in NH(OH)N(O)OH undergoes cleavage to generate HONO and HNO, giving TS14. The other group involves pathways that progress *via* $NH_2(O)NO_2$. $NH(OH)NO_2$ transitions to $NH_2(O)NO_2$ by intramolecular H transfer from an −OH to an —NH_2 group to give TS13. The decomposition of $NH_2(O)NO_2$ has already been discussed above. The presence of water assists both reactions leading to TS12 and TS14. The intramolecular H transfer reaction R17 has a very large energy barrier of 233.1 kJ/mol, and this reaction requires the presence of water to proceed.

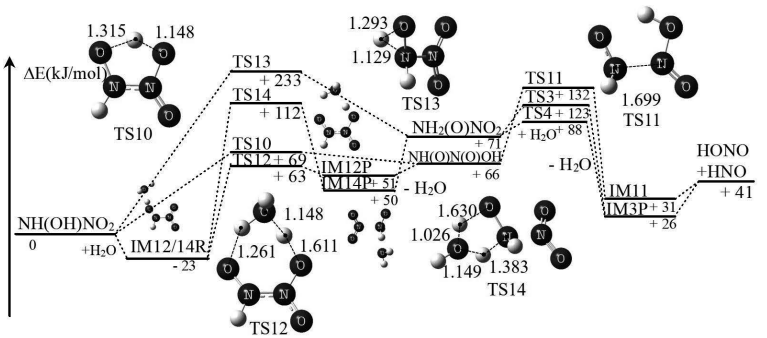

Figure 7. Potential energy profiles* for the decomposition of the intermediate $NH(OH)NO_2$

*The energy profiles were calculated at the CBS-QB3//ωB97XD/6-311++G(d,p)/SCRF = (solvent = water) level of theory.

3.1.4 The self-decomposition of HNO_3

Two molecules of HNO_3 may decompose to yield N_2O_5 and H_2O as follows:

$$HNO_3 + HNO_3 \rightarrow N_2O_5 + H_2O \qquad \text{(R19)}$$

The same type of reaction in the gas phase was theoretically investigated previously [29]. We examined this self-decomposition reaction and the subsequent processes and Figure 8 depicts the potential energy profile and optimized structures. The energy barrier and heat of reaction were determined to be 89.8 kJ/mol. This reaction starts with a proton transfer from one HNO_3 to the other. The protonated $H_2NO_3^+$ subsequently decomposes to H_2O and NO_2^+ and the NO_2^+ binds to the deprotonated NO_3^- to form N_2O_5.

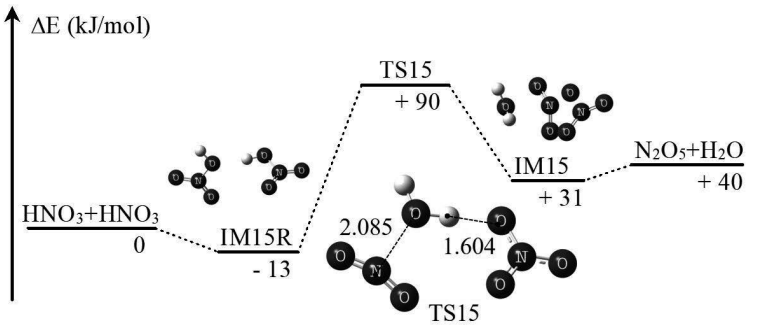

Figure 8. Potential energy profile* for the self-decomposition of HNO_3

*The energy profile was calculated at the CBS-QB3//ωB97XD/6-311++G(d,p)/SCRF = (solvent = water) level of theory

$$NH_2OH + N_2O_5 \rightarrow NH_2ONO_2 + HNO_3 \quad (R20)$$
$$NH_3OH^+ + N_2O_5 \rightarrow NH_2(OH)NO_2^+ + HNO_3 \quad (R21)$$

Figure 9 shows the potential energy profile for R20 and the optimized structures. The energy barrier was calculated as 27.5 kJ/mol. The neutral-neutral reaction of N_2O_5 and NH_2OH begins with the decomposition of N_2O_5 to NO_2 and NO_3, and the resulting NO_2 immediately combines with NH_2OH to form $NH_2(OH)NO_2$ as TS16. The NO_3 removes an H from $NH_2(OH)NO_2$ to yield $NH_2(O)NO_2$ and HNO_3. The $NH_2(O)NO_2$ decomposition process has already been discussed above.

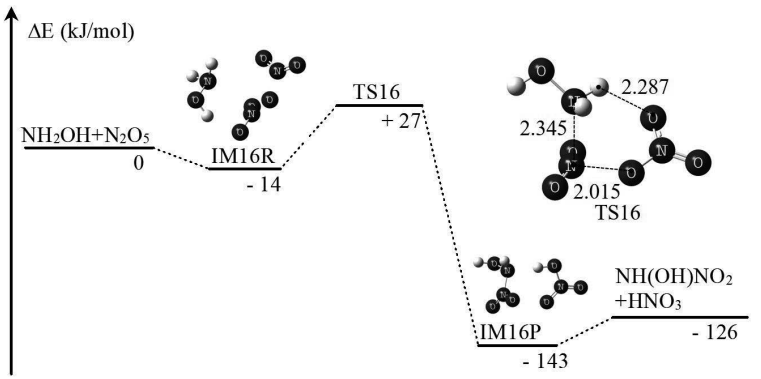

Figure 9. Potential energy profile* for the bimolecular reaction of NH_2OH and N_2O_5

*The energy profile was calculated at the CBS-QB3//ωB97XD/6-311++G(d,p)/SCRF = (solvent = water) level of theory.

Figure 10 depicts the potential energy profile for R21 along with the optimized structures. The energy barrier was determined to be 50.9 kJ/mol. The ion-neutral reaction of NH_3OH^+ and N_2O_5 starts with the decomposition of N_2O_5 to NO_2^+ and NO_3^-, which removes a proton from NH_3OH^+ to give HNO_3 and NH_2OH as TS17. The dissociated NO_2^+ combines with NH_2OH to yield $NH_2(OH)NO_2^+$. The decomposition of $NH_2(OH)NO_2^+$ has been discussed above.

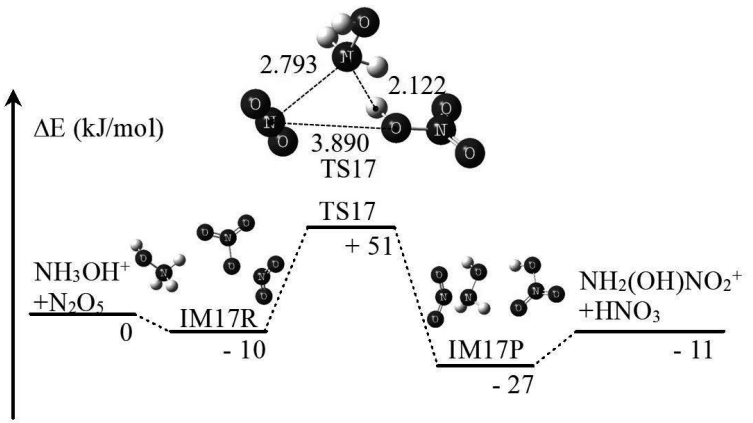

Figure 10. Potential energy profile* for the bimolecular reaction of NH_3OH^+ and N_2O_5

*The energy profile was calculated at the CBS-QB3//ωB97XD/6-311++G(d,p)/SCRF = (solvent = water) level of theory.

Because the energy barrier associated with R19 is higher than those for R20 and R21, the rate determining step is believed to be R19.

3.1.5 The reaction scheme of initial decomposition of HAN

The schemes below summarize the sets of reactions investigated in this study.

Scheme 1. Neutral-neutral reaction mechanism I

$HAN + H_2O \rightarrow NH_2OH + HNO_3 + H_2O$ (1)
$NH_2OH + HNO_3 \rightarrow NH_2(O)NO_2 + H_2O$ (R3)
$NH_2(O)NO_2 (+ H_2O) \rightarrow HNO + HONO (+ H_2O)$ (R4, R5)
$HAN \rightarrow HNO + HONO + H_2O$ (9)

Scheme 2. Neutral-neutral reaction mechanism II

$HAN + H_2O \rightarrow NH_2OH + HNO_3 + H_2O$ (1)
$NH_2OH \rightarrow NH_3O$ (10)
$NH_3O + HNO_3 \rightarrow NH_2ONO_2 + H_2O$ (R6)
$NH_2ONO_2 (+ H_2O) \rightarrow HNO + HONO (+ H_2O)$ (R7, R8)
$HAN \rightarrow HNO + HONO + H_2O$ (9)

Scheme 3. Ion-neutral reaction mechanism

$HAN \rightarrow NH_3OH^+ + NO_3^-$ (11)
$NH_3OH^+ + HNO_3 \rightarrow NH_2(OH)NO_2^+ + H_2O$ (R10)

$NH_2(OH)NO_2^+ + NO_3^- \rightarrow NH(OH)NO_2 + HNO_3$ (R13)
$NH(OH)NO_2$ (+ H_2O) → NH(O)N(O)OH (+ H_2O) (R14, R16)
NH(O)N(O)OH → HNO + HONO (R15)
HAN → HNO + HONO + H_2O (9)

Scheme 4. HNO_3 self-decomposition mechanism I
HAN + H_2O → NH_2OH + HNO_3 + H_2O (1)
$HNO_3 + HNO_3 \rightarrow N_2O_5 + H_2O$ (R19)
$N_2O_5 + NH_2OH \rightarrow NH_2(O)NO_2 + HNO_3$ (R20)
$NH_2(O)NO_2$ (+ H_2O) → HNO + HONO (+ H_2O) (R4, R5)
HAN → HNO + HONO + H_2O (9)

Scheme 5. HNO_3 self-decomposition mechanism II
HAN → $NH_3OH^+ + NO_3^-$ (11)
$HNO_3 + HNO_3 \rightarrow N_2O_5 + H_2O$ (R19)
$N_2O_5 + NH_3OH^+ \rightarrow NH_2(OH)NO_2^+ + HNO_3$ (R20)
$NH_2(OH)NO_2^+ + NO_3^- \rightarrow NH(OH)NO_2 + HNO_3$ (R13)
$NH(OH)NO_2$ (+ H_2O) → NH(O)N(O)OH (+ H_2O) (R14, R16)
NH(O)N(O)OH → HNO + HONO (R15)
HAN → HNO + HONO + H_2O (9)

Regardless of the mechanism, the overall initial decomposition reaction can be written using one formula: HAN → HONO + HNO + H_2O. The maximum energy barrier values were 124.8 kJ/mol (Scheme 1), 88.7 kJ/mol (Scheme 2), 91.7 kJ/mol (Scheme 3) and 89.8 kJ/mol (Schemes 4 and 5). With regard to the energy barriers, Schemes 2, 3, 4 and 5 are all plausible. In water, HAN is known to primarily dissociate into the ion pair NH_3OH^+ and NO_3^-, so the concentrations of NH_2OH and HNO_3 will be low. In addition, the concentration of NH_3O will be less than that of NH_2OH based on the constant for the equilibrium between NH_2OH and $^+NH_3O^-$ in aqueous solution: $K_T = ([^+NH_3O^-]/[NH_2OH]) = 2.6 \times 10^{-2}$ [26]. Therefore, we concluded that the ionic reaction represented by Scheme 3 is dominant during the initial HAN decomposition in a standard aqueous solution. However, the primary pathway will vary with the chemical states and concentrations of the species in HAN solutions. Under acidic conditions, for example, Scheme 5 might be more plausible than Scheme 3 due to the high concentration of HNO_3. Thus, these schemes should all be considered depending on the reaction conditions in order to develop an advanced reaction model capable of accurately predicting the combustion behaviour of this propellant system.

According to Lee and Litzinger [18], the activation energy, E_a, of the reaction

$NH_2OH + HNO_3 \rightarrow HONO + HNO + H_2O$ is 27.6 ±2.9 kJ/mol. This is much lower than the energy barrier values, ΔE_0, obtained from the present study. Lee and Litzinger obtained both E_a and frequency parameter values by an inverse analysis technique. Therefore, it is important to compare the magnitude of the rate coefficients. We calculated the rate coefficients using the transition state theory for the TSs and reactants investigated in this study. The rate coefficient from this study was much slower than the one from Ref. [18]. Detail kinetic modelling must be conducted in future work. Gowland and Stedman [30] experimentally obtained an E_a of 104.6 kJ/mol for the reaction between HNO_3 and NH_3OH^+ in aqueous solution. This value is in good agreement with our calculated ΔE_0 of 91.7 kJ/mol. According to Brill *et al*. [31], "While the E_a values reported for the decomposition of aqueous HAN under different conditions vary significantly, modest confidence can still be placed in the fact that higher concentrations of HAN yield E_a in the 60-70 kJ/mol range, but E_a values above 100 kJ/mol are possible for lower concentrations." In the future, the reaction pathways presented in this paper should therefore be validated by constructing a quantitative model and simulating the reaction behaviour of HAN/water solutions. The simulation will provide an explanation for variations in the activation energy under various conditions.

3.2 The catalytic decomposition of HAN/HONO

3.2.1 HONO + NH_2OH/NH_3OH^+ reactions

We identified and investigated both the neutral-neutral reaction of HONO and NH_2OH and the ion-neutral reaction of HONO and NH_3OH^+. Going from neutral NH_2OH and HONO molecules to products, two pathways were obtained, involving the following chemical reactions:

$$NH_2OH + HONO \rightarrow NH_2(O)NO + H_2O \text{ (TS18)} \quad \text{(R22)}$$
$$NH_2(O)NO \rightarrow 2HNO \text{ (TS19)} \quad \text{(R23)}$$
$$NH_2OH + HONO \rightleftharpoons [NH(OH)\text{-}ON] + H_2O \text{ (TS20)} \quad \text{(R24)}$$
$$[NH(OH)\text{-}ON] \rightleftharpoons 2HNO \text{ (TS21)} \quad \text{(R25)}$$

Figure 11 shows the potential energy diagram, including the optimized structures of the TSs and intermediate complexes of reactants and products for the neutral-neutral reaction of NH_2OH and HONO. In the mechanism that proceeds *via* TS18, hydrogen transfer from the OH group of NH_2OH to HONO triggers the bimolecular reaction and the H_2ONO with the added hydrogen subsequently dissociates to H_2O and NO *via* TS18, as shown in Figure 11. The dissociated

NO then combines with NH_2O to give $NH_2(O)NO$. The energy barrier to this process was calculated to be 74.9 kJ/mol.

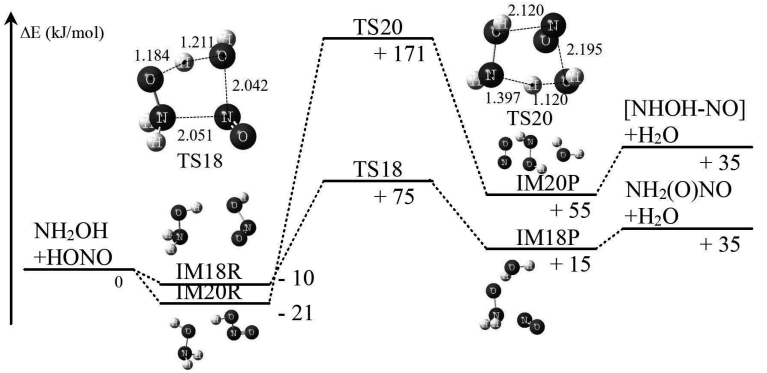

Figure 11. Potential energy* diagram for the HONO-NH_2OH reaction
*The energy profiles were calculated at the CBS-QB3//ωB97XD/6-311++G(d,p)/SCRF = (solvent = water) level of theory.

In the TS20 mechanism, the bimolecular reaction also starts with hydrogen transfer from NH_2OH to HONO, but the hydrogen dissociates from the NH_2 group in NH_2OH to give TS20 as shown in Figure 12. The HONO with the hydrogen subsequently dissociates to H_2O and NO, again *via* TS18. The energy barrier for this pathway was determined to be 171.2 kJ/mol. This value is much higher than that for R22 because the N−H bond is significantly stronger than the O−H bond. R24 and R25 are of less interest because the energy barrier for R24 is much higher than that for R22.

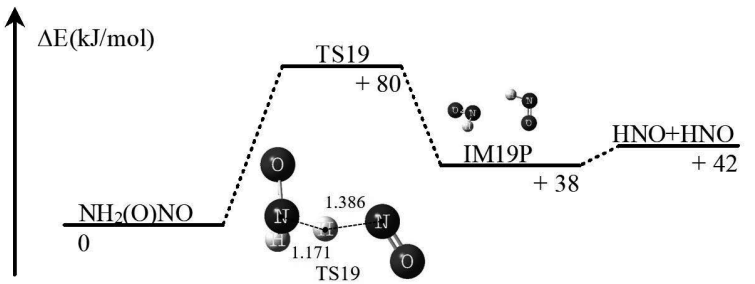

Figure 12. Potential energy* diagram for the decomposition of the intermediate $NH_2(O)NO$
*The energy profile was calculated at the CBS-QB3//ωB97XD/6-311++G(d,p)/SCRF = (solvent = water) level of theory.

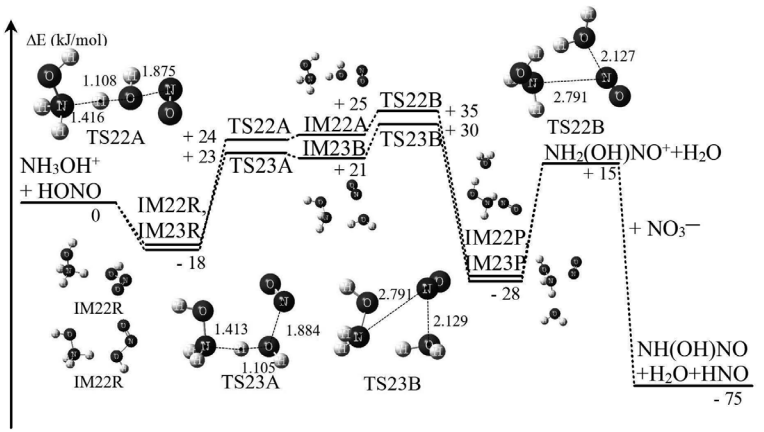

Figure 13. Potential energy* diagram for the bimolecular reaction of NH_3OH^+ and HONO

*The energy profiles were calculated at the CBS-QB3//ωB97XD/6-311++G(d,p)/SCRF = (solvent = water) level of theory.

We also identified and investigated $NH_2(O)NO$ decomposition through reaction R23. Figure 13 presents the potential energy diagram for the reaction and the optimized structures for the TS, reactant and products. Here $NH_2(O)NO$ decomposes to two HNO molecules by intramolecular hydrogen transfer that proceeds through TS2. The energy barrier was calculated to be 80.4 kJ/mol. The resulting HNO is known to decompose to N_2O and H_2O in an exothermic reaction [8]. This series can be summarized as a single global reaction:

$$NH_2OH + HONO \rightarrow N_2O + 2H_2O \quad (3)$$

In aqueous solution, HAN typically dissociates to form the ion pair NH_3OH^+ and NO_3^-. We therefore also identified and investigated reactions related to NH_3OH^+ as follows:

$$NH_3OH^+ + HONO \rightarrow NH_2(OH)NO^+ + H_2O \text{ (TS22 and 23)} \quad \text{(R26-R29)}$$
$$NH_2(OH)NO^+ + NH_2OH \rightarrow NH(OH)NO + NH_3OH^+ \quad \text{(R30)}$$
$$NH_2(OH)NO^+ + NO_3^- \rightarrow NH(OH)NO + HNO_3 \quad \text{(R31)}$$

Figure 14 shows the potential energy diagram and the optimized TSs and intermediates for this pathway. Both reactions begin with proton transfer from NH_3OH^+ to HONO, and the protonated HONO subsequently decomposes to H_2O and NO^+ *via* TS22A or TS23A. The reactions yield similar intermediate

complexes, $[NH_2OH\text{-}NO\text{-}H_2O]^+$, to IM5A and IM6A. These intermediate complexes rearrange such that NO^+ combines with NH_2OH to yield $NH_2(OH)NO^+$ as TS22B and TS23B. The rate determining steps appear to be R26 and R28 because these represent the highest energy barriers in this series of reactions: 23.6 kJ/mol and 22.6 kJ/mol, respectively. $NH_2(OH)NO^+$ can be deprotonated to NH(OH)NO by NO_3^- or NH_2OH, both of which are abundantly present in aqueous HAN solutions. This reaction eventually yields NH(OH)NO and H_2O with an exothermic heat of reaction of 106 kJ/mol. Because the associated reaction barriers are much lower than that for the decomposition, the exothermic reaction of NH_3OH^+ with HONO proceeds following the decomposition.

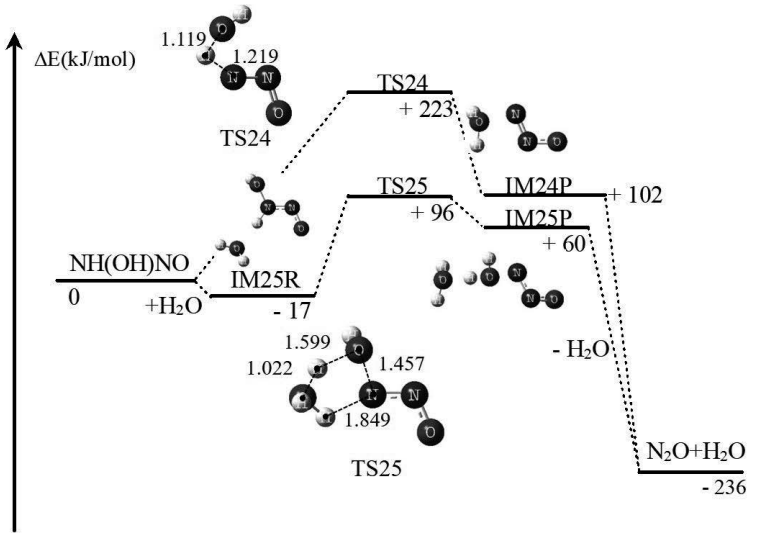

Figure 14. Potential energy* diagram for the decomposition of the intermediate $NH(OH)NO_2$

*The energy profiles were calculated at the CBS-QB3//ωB97XD/6-311++G(d,p)/SCRF = (solvent = water) level of theory.

This work also investigated the decomposition of the intermediate NH(OH)NO as follows:

$$NH(OH)NO\ (+ H_2O) \rightarrow N_2O + H_2O\ (+ H_2O)\ (TS24, TS25) \qquad (R32, R33)$$

Figure 15 presents the associated potential energy diagram and the optimized structures for the TSs and intermediates. Here, water molecules assist the reaction, acting as hydrogen-transfer agents. Although the unimolecular

decomposition of NH(OH)NO has a high energy barrier of 222.3 kJ/mol, the presence of water decreases the barrier to 95.8 kJ/mol. This series of reactions can be written as one global reaction:

$$NH_3OH^+ + HONO \rightarrow N_2O + H_2O + H_3O^+$$

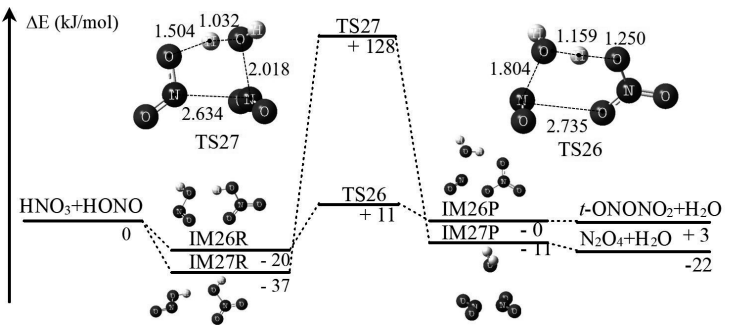

Figure 15. Potential energy* diagram for the HNO_3-HONO reaction
*The energy profiles were calculated at the CBS-QB3//ωB97XD/6-311++G(d,p)/SCRF = (solvent = water) level of theory.

3.2.2 HNO_3 + HONO reaction and t-$ONONO_2$ + NH_2OH/NH_3OH^+ reactions

HONO can react with not only NH_2OH but also HNO_3. This work therefore identified reactions in the HNO_3 + HONO system, the beginning of which can be represented by the following:

$$HNO_3 + HONO \rightarrow \textit{trans}\text{-}ONONO_2 + H_2O \text{ (TS26)} \quad \text{(R34)}$$
$$HNO_3 + HONO \rightarrow N_2O_4 + H_2O \text{ (TS27)} \quad \text{(R35)}$$

Figure 16 shows the potential energy diagram and the optimized TS and intermediate structures. The energy barrier for R34 was calculated to be 11.4 kJ/mol. The reaction starts with the dissociation of OH from HONO and a subsequent proton transfer from HNO_3 to HONO to give TS26. The dissociated NO^+ combines with NO_3^- to form *trans*-$ONONO_2$ (*t*-$ONONO_2$). R35 also involves a proton transfer, but from HONO to HNO_3 to produce TS27. The energy barrier for R35 was 128.5 kJ/mol, a value that is much higher than that for R34. This higher barrier occurs because HONO is a weaker acid than HNO_3. Consequently, R34 is much more likely than R35 on a thermodynamic basis.

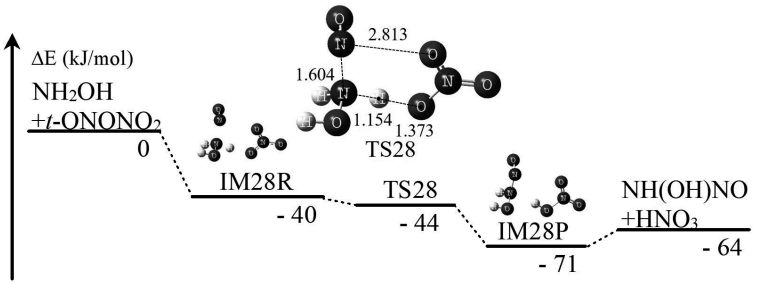

Figure 16. Potential energy* diagram for the *t*-$ONONO_2$ reaction with NH_2OH
*The energy profiles were calculated at the CBS-QB3//ωB97XD/6-311++G(d,p)/SCRF = (solvent = water) level of theory.

Following the formation of t-$ONONO_2$, there are two paths: a neutral reaction and an ionic reaction. We identified and investigated the following reactions:

$$NH_2OH + t\text{-}ONONO_2 \rightarrow NH(OH)NO + HNO_3 \text{ (TS28)} \quad \text{(R36)}$$
$$NH_3OH^+ + t\text{-}ONONO_2 \rightarrow NH_2(OH)NO^+ + HNO_3 \text{ (TS29)} \quad \text{(R37)}$$

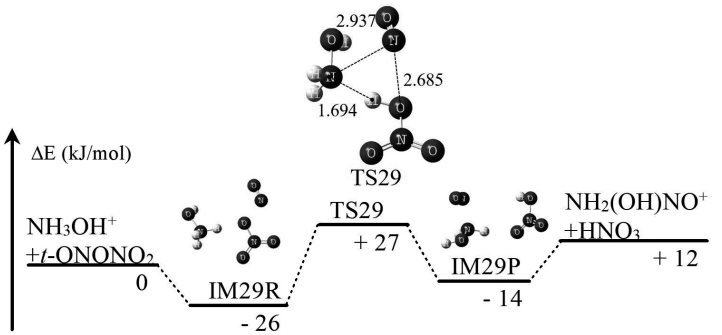

Figure 17. Potential energy* diagram for the reaction of *t*-$ONONO_2$ with NH_3OH^+
*The energy profiles were calculated at the CBS-QB3//ωB97XD/6-311++G(d,p)/SCRF = (solvent = water) level of theory.

Figure 17 presents the potential energy diagram for R36 and the optimized structures of the TS and intermediates. The neutral-neutral reaction of *t*-$ONONO_2$ and NH_2OH begins with the decomposition of *t*-$ONONO_2$ to NO^+ and NO_3^-, after which the dissociated NO^+ combines with NH_2OH to form $NH_2(OH)NO^+$, while the NO_3^- immediately abstracts a proton from $NH_2(OH)NO^+$ to yield NH(OH)NO and HNO_3 (as TS28), as shown in Figure 17. The potential energy diagram demonstrates that this reaction has no barrier, meaning that the reaction proceeds

exothermically to give NH(OH)NO and HNO_3 immediately after *t*-$ONONO_2$ has reacted with NH_2OH. The NH(OH)NO subsequently decomposes to N_2O and H_2O with a significant heat release, as in R32.

Figure 18 provides the potential energy diagram for R37 and the optimized TS and intermediate structures. The energy barrier height was determined to be 26.6 kJ/mol. The ionic reaction of NH_3OH^+ and *t*-$ONONO_2$ starts with a proton transfer from NH_3OH^+ to *t*-$ONONO_2$, after which the protonated *t*-$ONONO_2$ decomposes to HNO_3 and NO^+, and the NO^+ then combines with NH_2OH as TS29. The $NH_2(OH)NO^+$ is deprotonated to yield NH(OH)NO in an exothermic reaction series corresponding to R36 and R37.

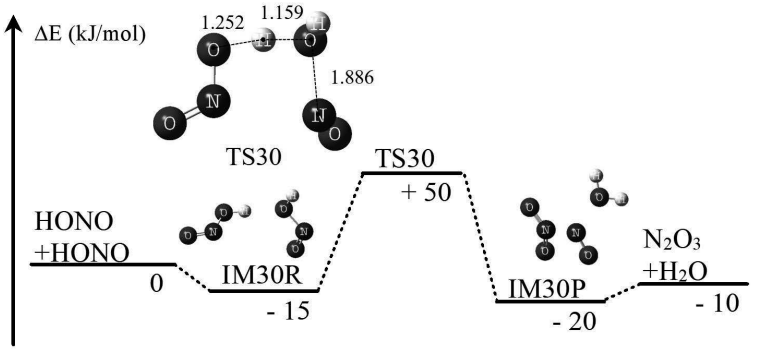

Figure 18. Potential energy* diagram for the self-decomposition reaction of HONO

*The energy profiles were calculated at the CBS-QB3//ωB97XD/6-311++G(d,p)/SCRF = (solvent = water) level of theory.

R36 and R37 have either no energy barrier or a lower barrier than R34 and therefore R34 is the rate determining step in this series of reactions.

3.2.3 HONO + HONO self-decomposition and N_2O_3 + NH_2OH/ NH_3OH^+ reactions

Two molecules of HONO may decompose to yield N_2O_3 and H_2O as follows:

$$HONO + HONO \rightarrow N_2O_3 + H_2O \text{ (TS30)} \qquad \text{(R38)}$$

We identified and investigated this self-decomposition reaction and Figure 19 shows the potential energy diagram and the associated optimized structures. The energy barrier and heat of reaction were calculated to be 50.4 kJ/mol. This reaction is initiated by a proton transfer from one HONO to the other. The

protonated H_2ONO^+ decomposes to H_2O and NO^+ and the NO^+ then combines with ONO^- to form N_2O_3.

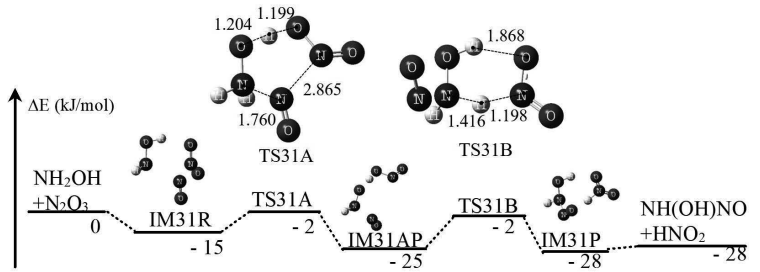

Figure 19. Potential energy* diagram for the reaction of N_2O_3 with NH_2OH
*The energy profiles were calculated at the CBS-QB3//ωB97XD/6-311++G(d,p)/SCRF = (solvent = water) level of theory.

After the formation of N_2O_3, there are two possible paths: a neutral reaction and an ionic reaction that is the same as the one that follows the formation of *t*-$ONONO_2$. We identified and investigated reactions related to N_2O_3 as shown below.

$$NH_2OH + N_2O_3 \rightarrow NH_2ONO + HONO \text{ (TS31)} \qquad \text{(R39, R40)}$$
$$NH_3OH^+ + N_2O_3 \rightarrow NH_2(OH)NO^+ + HONO \text{ (TS32)} \qquad \text{(R41, R42)}$$

Figure 20 presents the potential energy diagram for R39 and R40, and the optimized structures of the TSs and intermediates for these pathways. The neutral reaction of N_2O_3 and NH_2OH starts with the decomposition of N_2O_3 to NO_2 and NO, after which the NO_2 immediately abstracts a hydrogen from NH_2OH to form $NH_2(O)NO$ and HONO as TS31A. The dissociated NO combines with NH_2O to form NH(OH)NO and HNO_2 as TS31B. The $NH_2(O)NO$ decomposes to two HNO molecules according to R23. The potential energy diagram shows that this reaction has no barrier. Therefore this exothermic reaction proceeds immediately to yield NH(OH)NO and HNO_2 once N_2O_3 has attacked NH_2OH.

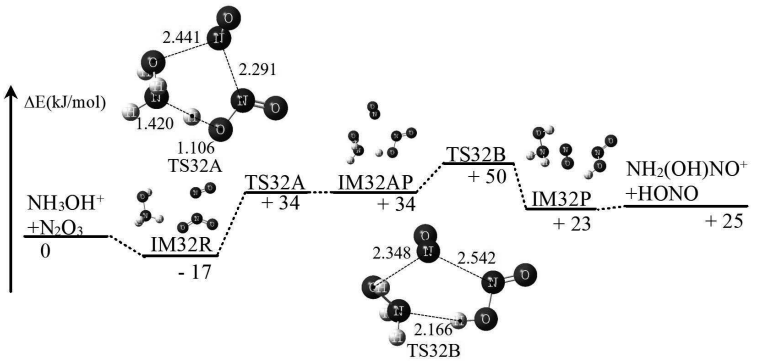

Figure 20. Potential energy profiles* for the reaction of N_2O_3 with NH_3OH^+
*The energy profiles were calculated at the CBS-QB3//ωB97XD/6-311++G(d,p)/SCRF = (solvent = water) level of theory.

Figure 11 shows the potential energy diagram for R41 and R42, and the optimized structures. The maximum energy barrier was calculated to be 33.9 kJ/mol. The ionic reaction of NH_3OH^+ and N_2O_3 starts with the decomposition of N_2O_3 to NO^+ and NO_2^-, after which the dissociated NO_2^- abstracts a proton from NH_3OH^+ to yield HONO and NH_2OH as TS32A. The dissociated NO^+ combines with NH_2OH to form $NH_2(OH)NO^+$. R39-40 and R41-42 have either no energy barrier or a lower barrier than R38. We therefore concluded that R38 is the rate determining step in this series of reactions.

3.2.4 Reaction scheme of HAN/HONO catalytic decomposition

Various sets of HONO-catalyzed reactions were investigated in this study based on the above results. We divided the HAN-HONO reactions into three groups according to the oxidizer that attacks NH_2OH or NH_3OH^+. These oxidizers were: HONO (Schemes 1 and 2), *t*-$ONONO_2$ (Schemes 3 and 4) and N_2O_3 (Schemes 5 and 6). We additionally divided each scheme into two sub-schemes based on the target reductant, either neutral NH_2OH or ionic NH_3OH^+, to obtain six types of schemes.

Scheme 1. HONO-NH_2OH system reactions

$$NH_2OH + HONO \rightarrow NH_2(O)NO + H_2O \quad \text{(R22)}$$

$$NH_2(O)NO \rightarrow HNO + HNO \quad \text{(R23)}$$

$$HNO + HNO \rightarrow N_2O + H_2O \quad (4)$$

$$NH_2OH + HONO \rightarrow N_2O + 2H_2O \quad (3)$$

Scheme 2. $HONO\text{-}NH_3OH^+$ system reactions

$NH_3OH^+ + HONO \rightarrow NH_2(OH)NO^+ + H_2O$ (R26-29)
$NH_2(OH)NO^+ + NO_3^- \rightarrow NH(OH)NO + HNO_3$ (R31)
$NH_2OH + HNO_3 \rightarrow NH_3OH^+ + NO_3^-$ (10)
$NH(OH)NO\ (+ H_2O) \rightarrow N_2O + H_2O\ (+ H_2O)$ (R32, 32)
$NH_2OH + HONO \rightarrow N_2O + 2H_2O$ (3)

Scheme 3. *t*-$ONONO_2\text{-}NH_2OH$ system reactions

$HNO_3 + HONO \rightarrow t\text{-}ONONO_2 + H_2O$ (R34)
$t\text{-}ONONO_2 + NH_2OH \rightarrow NH(OH)NO + HNO_3$ (R40)
$NH(OH)NO\ (+ H_2O) \rightarrow N_2O + H_2O\ (+ H_2O)$ (R11, 12)
$NH_2OH + HONO \rightarrow N_2O + 2H_2O$ (3)

Scheme 4. *t*-$ONONO_2\text{-}NH_3OH^+$ system reactions

$HNO_3 + HONO \rightarrow t\text{-}ONONO_2 + H_2O$ (R34)
$t\text{-}ONONO_2 + NH_3OH^+ \rightarrow NH_2(OH)NO^+ + HNO_3$ (R41)
$NH_2(OH)NO^+ + NH_2OH \rightarrow NH(OH)NO + NH_3OH^+$ (R31)
$NH(OH)NO\ (+ H_2O) \rightarrow N_2O + H_2O\ (+ H_2O)$ (R32, 33)
$NH_2OH + HONO \rightarrow N_2O + 2H_2O$ (3)

Scheme 5. $N_2O_3\text{-}NH_2OH$ system reactions

$HONO + HONO \rightarrow N_2O_3 + H_2O$ (R38)
$N_2O_3 + NH_2OH \rightarrow NH(OH)NO + HNO_2$ (R39-40)
$HNO_2 \rightarrow HONO$ (11)
$NH(OH)NO\ (+ H_2O) \rightarrow N_2O + H_2O\ (+ H_2O)$ (R32, 33)
$NH_2OH + HONO \rightarrow N_2O + 2H_2O$ (3)

Scheme 6. $N_2O_3\text{-}NH_3OH^+$ system reactions

$HONO + HONO \rightarrow N_2O_3 + H_2O$ (R38)
$N_2O_3 + NH_3OH^+ \rightarrow NH_2(OH)NO^+ + HONO$ (R39, R40)
$NH_2(OH)NO_2^+ + NO_3^- \rightarrow NH(OH)NO_2 + HNO_3$ (R34)
$NH(OH)NO\ (+ H_2O) \rightarrow N_2O + H_2O\ (+ H_2O)$ (R32, 33)
$NH_2OH + HONO \rightarrow N_2O + 2H_2O$ (3)

Adding both sides of Schemes 1 to 6 and cancelling the intermediates, the global reaction for each of these can be written as a single reaction: $NH_2OH + HONO \rightarrow N_2O + 2H_2O$. In Schemes 1 and 2, HONO directly attacks NH_2OH or NH_3OH^+ to yield N_2O and H_2O (or H_3O^+) and the energy barriers for the rate determining steps were 74.9 kJ/mol (R22) and 22.6 kJ/mol (R26),

respectively. In Schemes 3 and 4, HONO attacks HNO_3 to give *t*-$ONONO_2$ and this compound subsequently attacks NH_2OH or NH_3OH^+ to form N_2O and H_2O (or H_3O^+). The energy barrier for the rate determining step in Schemes 3 or 4 was 11.4 kJ/mol (R34). Schemes 5 and 6 involve the decomposition of two HONO molecules to yield N_2O_3, with the N_2O_3 attacking NH_2OH or NH_3OH^+ to generate N_2O and H_2O (or H_3O^+). The energy barrier for the rate determining step in Schemes 5 or 6 was 50.4 kJ/mol (R17). Schemes 3 and 4 are therefore the most likely based on a consideration of the energy barrier heights for all of the schemes. According to Lee and Litzinger [18], the activation energy of the reaction $NH_2OH + HONO \rightarrow N_2O + H_2O$ is 13.8 ±0.8 kJ/mol. This E_a value is in good agreement with the determined for R34 (11.4 kJ/mol). Thus, we concluded that either Scheme 3 or Scheme 4 is dominant in the reactions of the HAN/HONO system.

4 Conclusions

The decomposition pathway of HAN in aqueous solution was investigated on the basis of *ab initio* calculations performed at the ωB97XD/6-311++G(d,p)/SCRF = (solvent = water) and CBS-QB3//ωB97XD/6-311++G(d,p)/SCRF = (solvent = water) levels of theories.

Mechanisms for the charge neutral-neutral bimolecular reactions ($NH_2OH + HNO_3 \rightarrow HNO + HONO + H_2O$ and $NH_3O + HNO_3 \rightarrow HNO + HONO + H_2O$), ion-neutral bimolecular reaction ($NH_3OH^+ + HNO_3 \rightarrow HNO + HONO + H_2O + H^+$) and HNO_3 self-decomposition ($HNO_3 + HNO_3 \rightarrow N_2O_5$) were developed. The maximum energy barrier for each of these reactions were calculated as 124.8 kJ/mol, 88.7 kJ/mol, 91.7 kJ/mol and 89.8 kJ/mol, respectively. Each of these reaction schemes appears to be thermodynamically viable and all yield the same products. The overall initial decomposition reaction can be summarized using a single equation: $HAN \rightarrow HONO + HNO + H_2O$. The primary scheme will depend on the concentrations of the various species in the reaction solution. HAN dissociates to form ion pairs in water, with NH_3OH^+ and NO_3^- being the major species. Therefore, we concluded that the $NH_3OH^+ + HNO_3$ reaction mechanism is dominant during the initial HAN decomposition in aqueous solution. The associated energy barrier of 91.7 kJ/mol is in good agreement with the activation energy reported in a previous study [31].

The HAN/HONO catalytic decomposition pathways following the initial decomposition of HAN were investigated based on density functional theory calculations. These calculations were performed at the same levels of theory.

We developed six mechanisms and each of these schemes provided the same global reaction: $NH_2OH + HONO \rightarrow N_2O + 2H_2O$. These schemes can be classed according to the combinations of oxidizers (HONO, *t*-$ONONO_2$ or N_2O_3) and reductants (NH_2OH or NH_3OH^+). In the HONO oxidizing scheme, HONO directly attacks NH_2OH or NH_3OH^+ to yield N_2O and H_2O (or H_3O^+) (= 171.2 kJ/mol or 74.9 kJ/mol respectively). In the *t*-$ONONO_2$ scheme, HONO reacts with HNO_3 to give *t*-$ONONO_2$ (= 11.4 kJ/mol) and the *t*-$ONONO_2$ oxidizes NH_2OH or NH_3OH^+ (= −44.8 kJ/mol or 22.6 kJ/mol respectively). In the N_2O_3 mechanism, two HONO molecules decompose to yield N_2O_3 (= 50.4 kJ/mol) and the N_2O_3 oxidizes NH_2OH or NH_3OH^+ (= −1.7 kJ/mol or 33.9 kJ/mol, respectively). Based on the energy barrier results, the *t*-$ONONO_2$ oxidizing scheme is the most plausible.

References

[1] Gohardani, A. S.; Stanojev, J.; Demairé, A.; Anflo, K.; Persson, M.; Wingborg, N.; Nilsson, C. Green Space Propulsion: Opportunities and Prospects. *Progress in Aerospace Sciences* **2014**, *71*: 128-149.

[2] Fukuchi, A. B.; Nagase, S.; Maruizumi, H.; Ayabe, M. HAN/HN-Based Monopropellant Thrusters. *IHI Engineering Review* **2010**, *43*: 22-28.

[3] Katsumi, T.; Kodama, H.; Matsuo, T.; Ogawa, H.; Tsuboi, N.; Hori, K. Combustion Characteristics of a Hydroxylammonium Nitrate Based Liquid Propellant. Combustion Mechanism and Application to Thrusters. *Combust. Explos. Shock Waves (Engl. Transl.)* **2009**, *45*: 442-453.

[4] Kondrikov, B. N.; Annikov, V.; Egorshev, Y.; deLuca, L. T. Burning of Hydroxylammonium Nitrate. *Combust. Explos. Shock Waves (Engl. Transl.)* **2000**, *36*: 135-145.

[5] Katsumi, T.; Kodama, H.; Ogawa, H.; Tsuboi, N.; Hori, K. Combustion Characteristics of HAN-based Liquid Propellant. *Sci. Tech. Energ. Mater*. **2009**, *70*: 27-32.

[6] Katsumi, T.; Inoue, T.; Nakatsuka, J.; Hasegawa, K.; Kobayashi, K.; Sawai, S.; Hori, K. HAN-Based Green Propellant, Application, and Its Combustion Mechanism. *Combust, Explos, Shock Waves (Engl. Transl.)* **2012**, *48*: 536-543.

[7] Pan, Y.; Yu, Y.; Zhou, Y.; Lu, X. Measurement and Analysis of the Burning Rate of HAN-based Liquid Propellants. *Propellants Explos. Pyrotech*. **2012**, *37*: 439-444.

[8] Lee, H.; Litzinger, T. A. Thermal Decomposition of HAN-Based Liquid Propellants. *Combust. Flame* **2001**, *127*: 2205-2222.

[9] Courthéoux, L.; Amariei, D.; Rossignol, S.; Kappenstein, C. Thermal and Catalytic Decomposition of HNF and HAN Liquid Ionic as Propellants. *Applied Catalysis B*: *Environmental* **2006**, *62*: 217-225.

[10] Amrousse, R.; Katsumi, T.; Bachar, A.; Brahmi, R.; Bensitel, M.; Hori, K. Chemical Engineering Study for Hydroxylammonium Nitrate Monopropellant Decomposition over Monolith and Grain Metal-based Catalysts. *Reac. Kinet. Mech. Cat*. **2013**, *111*: 71-88.

[11] Chang, Y. P.; Kuo, K. K. Assessment of Combustion Characteristics and Mechanisms of a HAN-Based Liquid Monopropellant. *Proc. AIAA/ASME/SAE/ ASEE Joint Propulsion Conf. and Exibit* (AIAA Paper No. 2001-3272), Salt Lake City, USA, July 8-11, **2001**.

[12] Harlow, D. G.; Felt, R. E.; Agnew, S.; Barney, G. S.; McKibben, J. M.; Garber, R.; Lewis, M. *Technical Report on Hydroxylamine Nitrate*. U. S. Department of Energy, **1998**.

[13] Wei, C.; Rogers, W. J.; Mannan, M. S. Thermal Decomposition Hazard Evaluation of Hydroxylamine Nitrate. *J. Hazard. Mater* **2006**, *130*: 163-168.

[14] Liu, L.; Wei, C.; Guo, Y.; Rogers, W. J.; Mannan, M. S. Hydroxylamine Nitrate Self-catalytic Kinetics Study with Adiabatic Calorimetry. *J. Hazard. Mater* **2009**, *162*: 1217-1222.

[15] Khare, P.; Yang, V.; Meng, H.; Risha, G. A.; Yetter, R. A. Thermal and Electrolytic Decomposition and Ignition of HAN-Water Solution. *Combust. Sci. Technol*. **2015**, *187*: 1065-1078.

[16] Khare, P. *Decomposition and Ignition of HAN-based Monopropellants by Electrolysis*. M.S. Thesis, Pennsylvania State University, **2009**.

[17] Thakre, P.; Duan, Y.; Yang, V. Modeling of Ammonium Dinitramide (ADN) Monopropellant Combustion with Coupled Condensed Phase and Gas Phase Kinetics. *Combust. Flame* **2014**, *161*: 347-362.

[18] Lee, H.; Litzinger, T. A. Chemical Kinetic Study of HAN Decomposition. *Combust. Flame* **2003**, *135*: 151-169.

[19] Oxley, J. C.; Brower, K. R. Thermal Decomposition of Hydroxylamine Nitrate. *Proc. SPIE 0872, Propulsion*, 63, May 9, **1988**.

[20] Klein, N. Ignition and Combustion of the HAN-based Liquid Propellants. *Proc. 27th JANNAF Combustion Subcommittee Meeting*, Vol. 1. CPIA Publication, November 5-9, Cheyenne, USA **1990**, 443-450.

[21] Chai, J. D.; Head-Gordon, M. Long-range Corrected Hybrid Density Functionals with Damped Atom-Atom Dispersion Corrections. *Phys. Chem. Chem. Phys*. **2008**, *10*: 6615-6620.

[22] Frisch, M. J.; Trucks, G. W.; Schlegel, H. B.; Scuseria, G. E.; Robb, M. A.; Cheeseman, J. R.; Scalmani, G.; Barone, V.; Mennucci, B.; Petersson, G. A.; Nakatsuji, H.; Caricato, M.; Li, X.; Hratchian, H.P.; Izmaylov, A.F.; Bloino, J.; Zheng, G.; Sonnenberg, J.L.; Hada, M.; Ehara, M.; Toyota, K.; Fukuda, R.; Hasegawa, J.; Ishida, M.; Nakajima, T.; Honda, Y.; Kitao, O.; Nakai, H.; Vreven, T.; Montgomery, J. A.; Peralta, J. E.; Ogliaro, F.; Bearpark, M.; Heyd, J. J.; Brothers, E.; Kudin, K. N.; Staroverov, V. N.; Keith, T.; Kobayashi, R.; Normand, J.; Raghavachari, K.; Rendell, A.; Burant, J. C.; Iyengar, S. S.; Tomasi, J.; Cossi, M.; Rega, N.; Millam, J. M.; Klene, M.; Knox, J. E.; Cross, J. B.; Bakken, V.; Adamo, C.;

Jaramillo, J.; Gomperts, R.; Stratmann, R.E.; Yazyev, O.; Austin, A. J.; Cammi, R.; Pomelli, C.; Ochterski, J. W.; Martin, R. L.; Morokuma, K.; Zakrzewski, V. G.; Voth, G. A.; Salvador, P.; Dannenberg, J. J.; Dapprich, S.; Daniels, A. D.; Farkas, O.; Foresman, J. B.; Ortiz, J. V.; Cioslowski, J.; Fox, D. J. *Gaussian 09*. Revision D.01; Gaussian, Inc., Wallingford CT. **2010**.

[23] Montgomery, J. A.; Frisch, M. J.; Ochterski, J. W.; Petersson, G. A. A Complete Basis Set Model Chemistry. VI. Use of Density Functional Geometries and Frequencies. *J. Chem. Phys.* **1999**, *110*: 2822-2827.

[24] Cossi, M.; Scalman, G.; Rega, N.; Barone, V. New Developments in the Polarizable Continuum Model for Quantum Mechanical and Classical Calculations on Molecules in Solution. *J. Chem. Phys*. **2002**, *117*: 43-54.

[25] de Lima, G. F.; Piego, J. R.; Duarte, H. A. Stability of Hydroxylamine Isomers in Aqueous Solution: Ab initio Study Using Continuum, Cluster-continuum and Shells Theory of Solvation. *Chem. Phys. Lett*. **2011**, *518*: 61-64.

[26] Fernádez, M. I.; Canle, M.; García, M. V.; Santaballa, J. A. A Theoretical Analysis of the Acid-base Equilibria of Hydroxylamine in Aqueous Solution. *Chem. Phys. Lett*. **2010**, *490*: 159-164.

[27] Wang, Q., Wei, C.; Pérez, L. M.; Rogers, W. J.; Hall, H. B.; Mannan, M. S. Thermal Decomposition Pathways of Hydroxylamine: Theoretical Investigation on the Initial Steps. *J. Phys. Chem. A.* **2010**, *114*: 9262-9269.

[28] Wang, Q.; Mannan, M. S. Prediction of Thermochemical Properties for Gaseous Ammonia Oxide. *J. Chem. Eng. Data* **2010**, *55*: 5128-5132.

[29] Alecu, I. M.; Marshall, M. Computational Study of the Thermochemistry of N_2O_5 and the Kinetics of the Reaction $N_2O_5+H_2O\rightarrow 2HNO_3$. *J. Phys. Chem. A* **2014**, *118*: 11405-11416.

[30] Gowland, R. J.; Stedman, G. Kinetic and Product Studies on the Decomposition of Hydroxylamine in Nitric Acid. *J. Inorg. Nucl. Chem*. **1981**, *43*: 2859-2862.

[31] Schoppelrei, J. W.; Kieke, M. L.; Brill, T. B. Spectroscopy of Hydrothermal Reactions. 2. Reactions and Kinetic Parameters of $[NH_2OH]NO_3$ and Equilibria of $(NH_4)_2CO_3$ Determined with a Flow Cell and FT Raman Spectroscopy. *J. Phys. Chem*. **1996**, *100*: 7463-7470.